

Main Measurement and Automation Nodes of Magnetic Nanoparticles Heater

Student project

Rostyslav P. Samchenko

Abstract—At carrying out the experiments to determine the losses for heating of magnetic nanoparticles (MNP) and composites on their basis, which are commonly used in the cancer treatment, it is necessary to reduce the number of manually regulated processes, e.g.: frequency change and resonance adjustment, alternating magnetic field strength amplitude change, as well as the measurements. In present article structural diagram of device for such purposes with improved automation level is presented and circuit engineering solutions for main measurement and automation nodes are proposed. There is an attempt to perform a purely electronic control of current flowing through the heating solenoid coil to adjust the magnetic field strength applied to the MNP sample without using any additional power electronics components.

Index Terms—Magnetic Nanoparticles, magnetic losses measurement, amplitude measurement, current control, induction heater, stepwise resonant frequency change

I. INTRODUCTION

IN the last decades magnetic nanoparticles (MNP) are of great interest for many researchers of wide range of disciplines. In particular, because of possibility of such materials to heat in the AC magnetic field due hysteresis and relaxation losses, they can be used for magnetic hyperthermia – the safely and efficient cancer treatment method [1]. With a temperature rise begins cancer cell death process. Below the 43°C temperature limit occurs only apoptosis – natural non-toxic programmable cell death mechanism [2]. The heating above it can cause the cell necrosis. So, it is necessary to conduct thorough laboratory testing to precisely define magnetic power loss curves of MNP. For such studies researchers put the experimental systems together using the separate modules, like induction heater, amplifier, variable capacitor, coil, measuring equipment etc. [1,3]. But such systems can have a low automation level, so the experiments can be carried out only in a presence of the qualified engineer, moreover, they can be very time-consuming.

Power of AC magnetic field dissipated by ball-shaped MNP per unit volume P can be described by a simplified equation[4]:

$$P = \pi\mu_0\chi_0 H_0^2 f \frac{2\pi f \tau}{1 + (2\pi f \tau)^2} \quad (1)$$

R.P. Samchenko is PhD-Student at Lviv Polytechnic National University, 79013 Lviv, Ukraine (e-mail: rostyslav.samchenko@gmail.com)

where μ_0 – magnetic permeability of free space, χ_0 – magnetic field dependent magnetic susceptibility, H_0 and f – amplitude and frequency of applied AC magnetic field, τ - effective relaxation time, which value is the range from 10^{-9} to 10^{-6} for 1 to 20 nm sized magnetite (Fe_3O_4) MNP [5].

Usually specific magnetic power losses P (W/kg) can be determined by calorimetric method by measuring MNP sample temperature rise ΔT over time Δt when sample is heated by magnetic field within the thermal insulation. Losses are then calculated by the formula based on [3]:

$$P = \phi c_s \left(\frac{\Delta T}{\Delta t} \right)_{t=0} \quad (2)$$

where ϕ – volume fraction of MNP in heated solution c_s -specific heat capacity of solution. Although there are other ways measure the magnetic losses (e.g. measuring the phase shift between the magnetic induction B and strength H [3]).

In such devices, to obtain high magnetic fields, solenoid coils as inductors are used, that (being connected to the capacitor) form resonant circuits. Using resonant circuit it is possible to pass through high AC current which has its maximum value at the resonant frequency of the LC-circuit.

In practice, the resonance frequency change can be achieved putting variable capacitor into LC-circuit. Adjusting the magnetic field strength can be done by changing the resonant circuit supply voltage manually (using variac or power amplifier).

In previous publications magnetic field distribution inside the coil and the optimum number of coil turns to ensure proper size of magnetic field uniformity area for evenly distributed sample heating was modeled [2] and a method of stepwise resonant frequency change was described, the advantage of which is that it can be implemented using only electronic components by switching in parallel to resonant circuit extra specially calculated capacitances [6].

II. OVERALL DEVICE STRUCTURE

The developed experimental system for determining magnetic losses for MNP heating has a structure that is shown in Fig. 1. As can be seen, there is calorimetric method of magnetic losses measurement implemented.

To exclude the influence of the magnetic field on the temperature measurement optical fiber thermometers should be used [2].

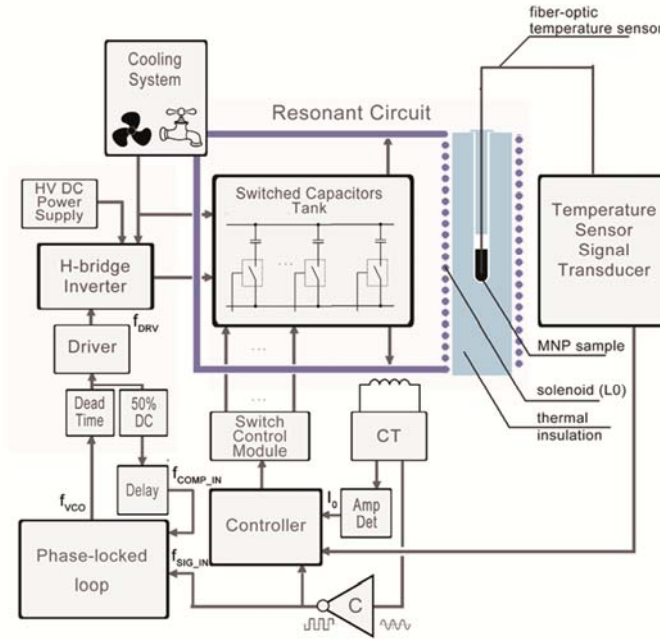


Fig. 1. Structure of developed experimental system for determining magnetic losses for MNP heating with improved automation level. DT – “dead time” circuit, CT – current transformer, AD – amplitude detector, C – comparator, 50%DC – duty cycle corr.

Since diagram of the system is quite cumbersome, only the main automation and measurement modules will be discussed in detail in present paper.

A. Resonant circuit structure

Based on research in [7], to reduce the current consumption, second order LC-circuit structure was chosen (Fig. 2). For measurement current flowing through the inductive branch the current transformer (CT) was used. The largest current in the circuit is achieved at zero of such resonant circuit i.e., the frequency of “series resonance” when the LC circuit resistance decreases.

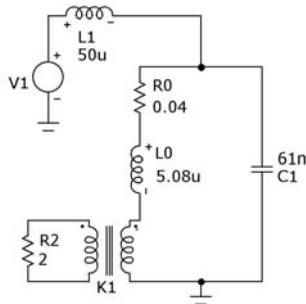


Fig. 2. Second order LC-circuit adjusted on series resonant frequency about 300 kHz with current transformer K1 in inductive branch

The angular frequency ω_0 of such circuit can be calculated as [8 p.199]:

$$\omega_0^2 = \frac{1}{L_1 C_1} + \frac{1}{L_0 C_1} \quad (3)$$

Hence, the resonant frequency f_0 :

$$f_0 = \frac{1}{2\pi\sqrt{C_1}} \sqrt{\frac{1}{L_1} + \frac{1}{L_0}} \quad (4)$$

where C_1 – effective capacitance of capacitive branches, L_0 – inductivity of the work coil, L_1 – inductivity of the matching coil.

On Fig. 3 typical amplitude response curve of current through L_0 and phase response curve of voltage on R_2 in CT secondary for circuit on Fig. 2 are presented.

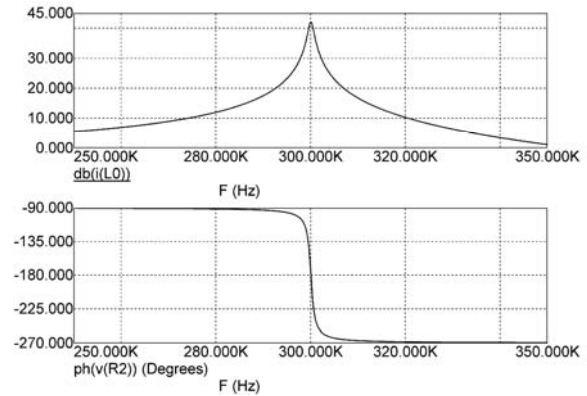


Fig. 3. Amplitude response curve of current through L_0 (top) and phase response curve of voltage on R_2 in CT secondary (bottom)

Inside the coil through which flows the current is forming magnetic field. As can be seen from the next formula, the magnetic field strength amplitude H_0 inside the coil is proportional to the amplitude of the current through work coil I_{L_0} and has the same frequency[15]:

$$H(t) = \frac{i(t)N}{l} \quad (5)$$

where N – work coil (inductor) turns number and l – its axial length. Therefore, the regulation of H_0 , based on similar parameters of current through coil I_{L_0} can be also convenient.

B. Automatic resonance adjust

As can be seen, the construction of such system is similar to the induction heater design. Therefore, from the latter the phase-locked loop technology (PLL) was taken for automatic resonant frequency adjust.

Fig. 3 shows that the phase of voltage across the resistor R_2 in transformer secondary passes through -180° at resonance. Due this condition, the PLL system can automatically adjust LC-circuit to the resonance by changing its output frequency so that the difference between the signals at its inputs is at minimum.

Fig. 4 shows the PLL implemented on a chip CD4046 with some additional elements and filter. Components C_1 , R_1 , R_2 on the Fig. 4 are chosen to provide frequency capture range from 50 to 400 kHz. V_2 is the output of comparator with signal inversion C. The output signal operates at the voltage-controlled oscillator output pin VCO_OUT.

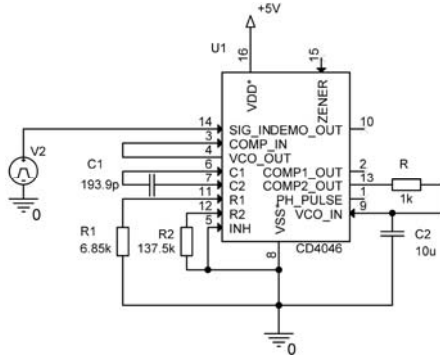


Fig. 4. PLL providing frequency capture range from 50 to 400 kHz

In designed system (Fig. 1) there is in the feedback loop, between the output VCO_OUT and the input COMP_IN, a dead time circuit and signal delay compensation circuit. The design of both is described in [9]. Using delay circuit VCO output signal is delayed for the time needed for signal passing from the VCO output to another input (SIG_IN) (Fig. 1).

C. Power supply for resonant circuit

The voltage supply of resonant circuit is also quite typical for induction heater: constant voltage of a power supply is fed to the MOSFET H-bridge inverter. Inverter is driven by the popular driver IC IR2110. The signal from the PLL passes to the input system with "dead time" pause of about 500 ns established using signal front delay circuit for the safe inverter bridge transistors opening. The output frequency of PLL f_{VCO_OUT} = output inverter frequency f_{INV} = input resonant circuit frequency f_{LC} .

D. Current transformer

High current through L_0 coil is scaled by CT with current transform ratio 100:1. In the CT secondary is placed resistor R_2 (Fig. 2) from which are taken separately the voltage drop signal amplitude (using amplitude detector AD) and frequency (using a comparator).

CT is designed to minimize phase δ_1 and current f_1 errors. CT secondary is wound of litz wire on a round Epcos core R22.1x13.7x12.5 made from N87 material. The value of secondary winding burden resistor R_2 is 1 Ohm (Fig. 2). The current and phase errors were calculated by the method, based on the guidelines from [10 p. 57]. The error values for CT are: $f_1 = 0,12\%$ $\delta_1 = 1' 56,787''$ or 0.0005662 rad.

E. Amplitude detector

Specifically for this task analog amplitude detector (AD) on low-cost components that operates at frequencies from 50 to 400 kHz was designed, covering the entire PLL capture range (Fig. 5). This paper presents an improved scheme of AD compared to [14], which has been already tested in practice. Elements at the input of U1.2 are changed from circuit based at integrating circuit into simple differentiating circuit that performs the same function of passing through impulses from the output of U1.1 to the U1.2 input.

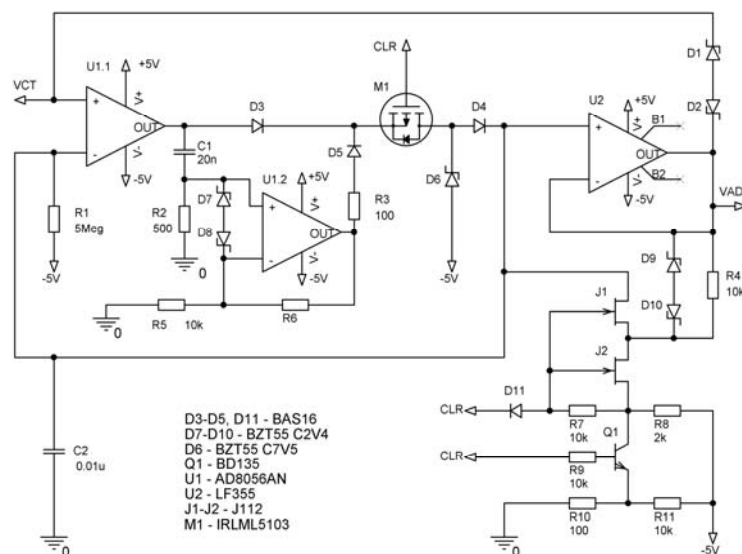


Fig. 5. Improved amplitude detector with raised upper operating frequency and external reset capability (VCT – input signal, VAD – output signal, CLR – external reset signal)

By AD practical implementation an error was found in the scheme presented in [14] – the absence of resistor to provide the input current path for the correct operation of the operational amplifier, because of bipolar transistors at its input stage.

After eliminating that problem first workability test of the developed AD device succeeded.

For improved amplitude detector the upper operating frequency was raised to 400 kHz and also added the external reset capability CLR +15 V. The lower frequency prototype of proposed AD is described in [11 p. 218]. To improve the speed the input amplifier LF355 was replaced by another low-cost dual amplifier AD8056 with high slew rate (1400 V/ μ s at unity gain). U1.1 - input amplifier which compares CT secondary winding burden resistor voltage V_{CT} with amplitude storing capacitor voltage C_2 . U1.2 used to gain U1.1 the current and to reduce negative errors due to U1.1 finite gain. Sample time is equal to $\frac{1}{4}$ detector signal period and during the first time after sampling there is a gradual error decrease to its negative value, where it takes its typical absolute value. Typical behavior of error ΔU_{AD} after the measurement is shown in Fig. 6 In case of positive errors, it is needed some time for capacitor C_2 discharging by opamp U1.1 input bias current to the value at which the error takes negative sign.

At a certain threshold value negative error output signal OP U1.1 - U1.2 is positive and passes through the diodes, charging C_2 . Due negative discharge voltage (-0.05 V set by voltage divider on R10-R11) detector has better threshold sensitivity to lower amplitudes. Output signal range: $V_{AD} = 0 \dots 1$ V. The AD output signal is fed to the ADC placed in microcontroller. Reset occurs in a few signal cycles. Normalized error will be presented after the AD experimental investigations.

Since the circuit elements: C_2 type K71-7 polystyrene, diode D1 and transistors switch on J1-J2, chosen for a low leakage and opamp U3 has a low bias current, it is obvious that C_2 discharges generally due to the U1.1 bias current I_b impact as well as due the current trough resistor R1.

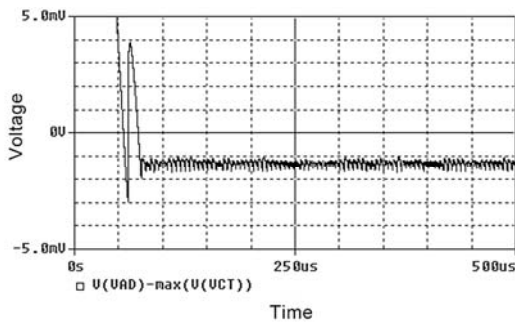


Fig. 6. Measurement error of amplitude detector simulation time domain at the output VAD of output buffer U2

III. CURRENT CONTROL

A. Stepwise resonant frequency change method

In the device was experimentally designed and being installed now the LC-circuit current control unit. By varying the resistance of analog switches that commute capacitances

of resonant circuit it is possible reduce its quality factor Q , and thus - the current in the circuit at resonance.

The present scheme uses 8 parallel switched branches (Fig. 7). These capacitive branches using the switching algorithm, described in [6], will result the 8 basic frequencies and additionally 6 intermediate frequencies, each of which is placed in the middle of the gap between the adjacent basic frequencies (Table 1).

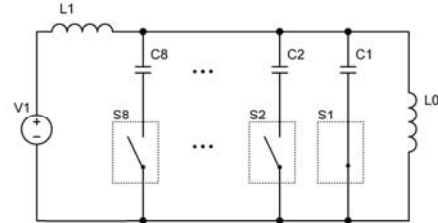


Fig. 7. Second order resonant circuit with switched capacitor branches

TABLE I
LIST OF CALCULATED RESONANT FREQUENCIES FOR CORRESPONDING ANALOG SWITCH COMBINATION ("1" – ON STATE, "0" – OFF STATE)

i	Combination of switches.	Resonant frequency, Hz	i	Combination of switches.	Resonant frequency, Hz
1	0000 0001	340000	9	0001 1111	166264
2	-	-	10	0010 1111	148581
3	0000 0011	300000	11	0011 1111	130899
4	0000 0101	277043	12	0101 1111	116523
5	0000 0111	254087	13	0111 1111	102149
6	0000 1011	231052	14	1011 1111	90734
7	0000 1111	208017	15	1111 1111	79320
8	0001 0111	187140	-	-	-

B. Inductor current control method (one switch case)

Each analog switch consists of two high-voltage high-current MOS transistors connected "source-to-source" for bipolar signal switching [12].

Switches are chosen with low channel on-resistance $r_{ds(on)}$ to minimize power losses and impact on quality factor of LC-circuit. A switch is driven by voltage 0-9 V, which is fed from the output of the photoelectric isolator (PVI), for example VOM1271, depending on input current of such IC.

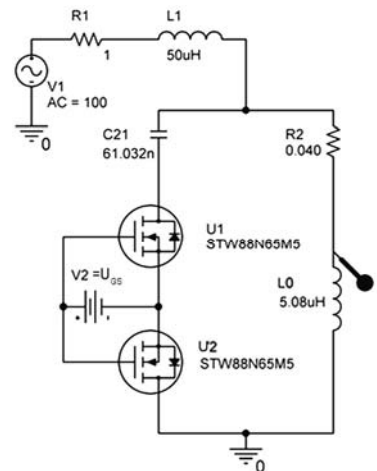


Fig. 8. LC-circuit with one capacitive branch consisting of capacitor and analog switch

As it is known, the maximum MOSFET channel current depends on the gate-source voltage U_{GS} , so with reduction of the control signal voltage (PVI input current), the resistance of the capacitive branch will increase, reducing the circuit quality factor Q and as a consequence - reducing the current in the circuit at resonance.

In Fig. 9 it is shown the dependence of the current through the coil I_{L0} at resonance on output voltage of PVI U_{GS} , which was obtained by simulation of the circuit on Fig. 8. (V_2 denotes switch U_{GS}) That can be used for purely electronic current magnitude control method.

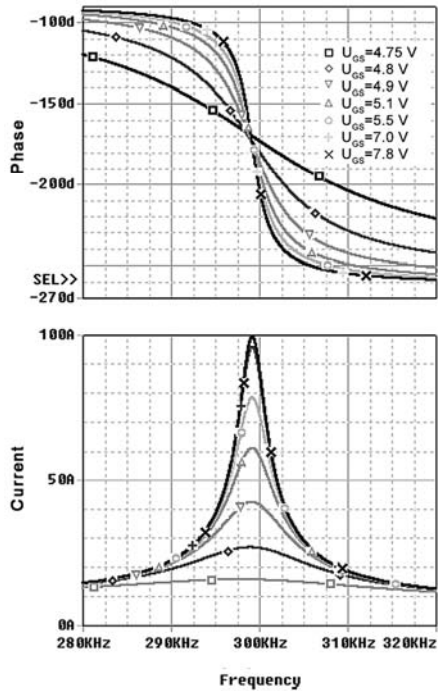


Fig. 9. Phase (top) and amplitude (bottom) response curves for different U_{GS}

C. Inductor current control method (multiple switch case)

To control the frequency it is needed to have at least few switches, as shown on Fig. 7. In this case, for current magnitude control by the Q-factor it is necessary to provide the same current through all PVI to hold all open switches U_{GS} voltages on one level.

It was specially designed this purpose switch control module (Fig. 10 and Fig. 11) that represents a current source with multi-output current mirror with switchable output branches. Current mirror is reflecting the input current to the corresponding switch PVI. Current source at the input is driven by DAC.

Switching LC-circuit capacitance branches occurs by turning off transistor base in corresponding mirror branches using logical signal transmitted from the MCU (V_1 and V_2 denote control bits on Fig. 11) input current of the current mirror I_{IN} is rejected into the output branches, causing all output currents $I_{OUT,N}$ to be equal. Differential amp loop operates to force the same amount of current to flow through the collector nodes of transistors Q_3 and Q_9 [13].

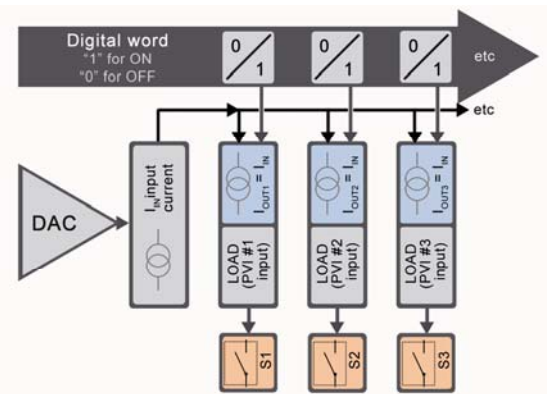


Fig. 10. Structural diagram of multi-output current mirror (CM) with DAC-controlled input current and switchable by logic signals mirror branches

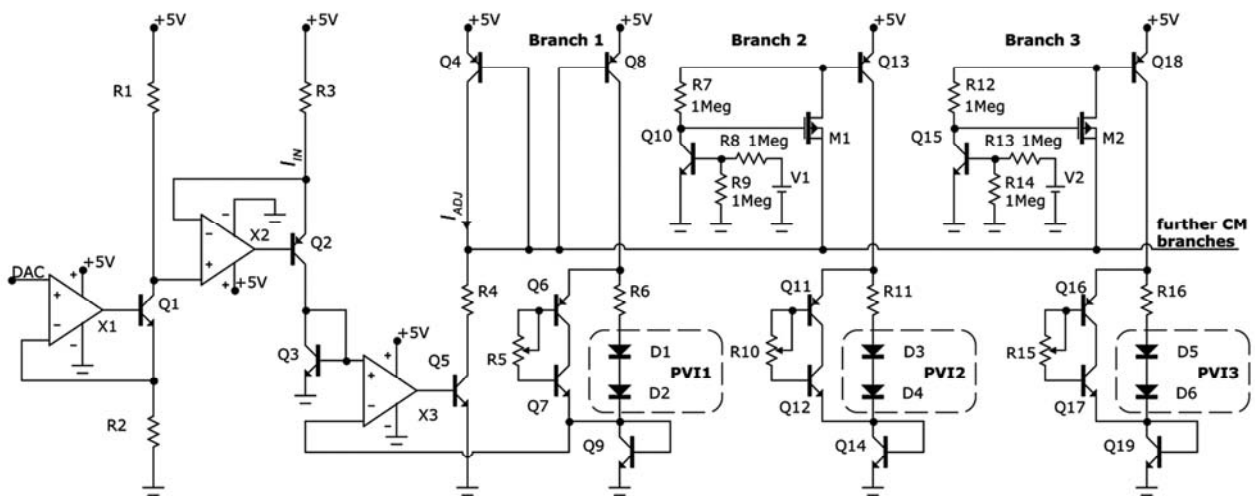


Fig. 11. Schematic of multi-output current mirror (CM) with DAC-controlled input current and switchable by logic signals mirror branches

The output current of operational amplifier X_3 affects the base current of Q_5 setting the current of transistor Q_4 that establishes the base-emitter voltage used in mirror transistors Q_8 , Q_{13} , Q_{18} .

Diode pairs (D_{1-2} ; D_{3-4} ; D_{5-6}) denote the input circuit of VOM1271T. Circuit on elements Q_{6-7} , Q_9 , D_{1-2} , R_6 , R_5 representing the load of CM's 1st output branch. The parallel branch on Q_{6-7} , R_5 is used for adjusting the PVI input current in this branch. The described branch load is same for all CM outputs. Using such method it is possible to adjust output current of each branch in the range from $\sim 0,5I_{IN}$ to $\sim 0,9I_{IN}$.

I_{IN} is set by the voltage controlled current source made on the operational amplifiers X_1 , X_2 , transistors Q_1 , Q_2 , and resistors R_1 , R_2 , R_3 . The input voltage of current source is defined by a microcontroller via digital-to-analog converter (DAC). Its output voltage represents on the Fig. 5 the 'DAC' node. The current I_{IN} is directly proportional to the DAC voltage set. The value of resistors R_1 , R_2 , R_3 selected to ensure the necessary variation range of I_{IN} for a full DAC voltage output range. X_1 , X_2 , X_3 should have rail-to-rail output operation capability.

Branches commutation occurs by switching bases of upper transistors Q_{13} , Q_{18} using p-channel MOSFET switches M_1 , M_2 . They are driven by IC PCA8574, which represents an 8-bit I2C bus expander. To the input of expander from the microcontroller transmits the serial digital word via I²C bus. Expander converts serial code into parallel and captures it on its outputs using latch registers.

Eight bits of expander output code can enable/disable the corresponding branch of the current mirror. Voltage sources V_1 and V_2 denote output bits of expander. Since outputs of IC PCA8574 implemented in CMOS logic, they cannot give high current for switching M_1 , M_2 , an additional transistor Q_5 , Q_6 in a source branch of M_1 , M_2 , described in [11 p. 586].

If a control output bit is LOW, transistor Q_5 is in cut-off mode, so p-channel transistor M_1 is closed. In this case through the corresponding branch of current mirror flows small current, so the respective VOM1271T gives too low voltage to open analog power switch in corresponding LC-circuit branch.

IV. CONCLUSION

The system with the presented structure can automatically adjust to the selected by the user experiment settings. Presented frequency control method allows its purely electronic control however, unlike in the method resonant frequency shift with variable capacitor, the frequency changes stepwise. Using the mentioned algorithm allows to get more frequencies than the capacitance branches amount in the LC-circuit. By controlling frequency through switching additional capacities it is available change current amplitude by altering capacitive part quality factor Q , without additional elements in the power part and resonant circuit. A special module placed in the optically isolated low-voltage control device part can affect the switches resistance by altering the voltage U_{DS} of

MOSFET switches. This dependence is nonlinear.

Designed CT and analog AD allow fast measurements of the current and performing its regulation using the controller. Additional filtering of input and output signals is needed because of output signal fluctuations seen at practice. The following publications will cover the results of AD tests.

First experiments confirmed current regulation methods, however due to switches overheating it is necessary to arrange their proper cooling. The results of practical implementation will be reported in the next publications.

REFERENCES

- [1] Tabatei S. N. (2009) Magnetic Nanoparticles Encapsulated in Hydrogel as Hyperthermic Actuators for Microrobots Designed to Operate in Vascular Network, *Intern. Conf. on Intell. Robots and Systems Proc.*, p. 546-551.
- [2] Samchenko R. (2012) "Heating and temperature measurement of magnetic nanoparticles based composites," *XIV Intern. PhD Workshop OWD*, Available: mechatronika.polsl.pl/owd/pdf2012/531.pdf
- [3] Beković M., Hamler A. (2012) "Experimental system for determining the magnetic losses of superparamagnetic materials; planning, realization and testing", *Applied Measurement Systems, InTech P.63-76*
- [4] Rosensweig, R.E. (2002) "Heating magnetic fluid with alternating magnetic field," *Journ. of Magnetism and Magnetic Materials*, Vol. 252, p. 370-374
- [5] Samchenko, R. (2012) "The use of mathematical models for approximate estimation induction heating magnetic nanoparticles" *Proc. of intern. Conf. "Recent directions of theoretical and applied researches 2012"*, Retrieved from: <http://sworld.com.ua/konfer26/128.pdf>
- [6] Samchenko R.P., Stadnyk B. I. (2013) "The method of LC-circuit stepwise resonant frequency change", *Sc. And prod. Journ. «Metrology and Instruments» Vol. 2/II(41)*, pp. 207-215
- [7] Burnett R. (2008) "High frequency induction heating," *Richie's Tesla Coil Webpage*, Available: <http://www.richieburnett.co.uk/indheat.html>
- [8] N.V. Zernov, V.H. Karpov (1965) Chapter IV: Resonant circuits under harmonic influence in *Teoriya radiotekhnicheskikh tsepey*, Moscow, pp. 159-220
- [9] Kухtetskyi S. (2011) Simple laboratory inverter for induction heating. Part 3, RAN, Retrieved from: <http://www.icct.ru/Practicality/Papers/27-01-2012/Archive/Invertor-07.pdf>
- [10] Afanasjev V. (1989) *Current transformers*, 2nd Edition, Leningrad, ISBN 5-293-04444-0
- [11] P. Horowitz, W. Hill (1989) *The Art of Electronics* 2nd Edition, Cambridge University Press, New York, 1125 p.
- [12] D.A. Dapkus (1994) Using MOS-Gated Power Transistor in AC Switch Applications Retrieved from: <http://www.irf.com/technical-info/designntp/dt94-5.pdf>
- [13] Craig N. Lambert (1997) Low-voltage multi-output current mirror circuit with improved power supply rejection mirrors and method therefor, US Patent 5625281 A
- [14] Samchenko R. (2013) "Automation level improvement of device for magnetic nanoparticles heating losses determination," *Conference Archives PTETiS XV International PhD Workshop OWD*, Wisla, Available: mechatronika.polsl.pl/owd/pdf2013/Samchenko_OWD_2013.pdf
- [15] Beković M., Trlep M. et al. (2013) „An experimental study of magnetic-field and temperature dependence on magnetic fluid's heating power," *Journ. of Magnetism and Magnetic Materials Vol. 331*, pp 261-268



Rostyslav P. Samchenko received M.Sc. degree in Metrology and Measuring Instruments at Lviv Polytechnic National University (Ukraine) and M.Sc. in Computer Engineering at Ilmenau University of Technology (Germany) in 2010. Currently pursuing the Ph.D. degree in Thermal Quantities Measuring Instruments and Methods at Lviv Polytechnic National University.